# Non-Equilibrium Adatom Thermal State Enables Rapid Additive Nanomanufacturing



| | |
|---|---|
| Journal: | *Physical Chemistry Chemical Physics* |
| Manuscript ID | CP-ART-03-2019-001478.R1 |
| Article Type: | Paper |
| Date Submitted by the Author: | 26-Apr-2019 |
| Complete List of Authors: | Henry, Matthew; Georgia Institute of Technology, Mechanical Engineering<br>Kim, Songkil; Pusan National University<br>Fedorov, Andrei; Georgia Institute of Technology George W Woodruff School of Mechanical Engineering; Georgia Institute of Technology, Parker H. Petit Institute for Bioengineering and Bioscience |
| | |

# Non-Equilibrium Adatom Thermal State Enables Rapid Additive Nanomanufacturing

*AUTHOR NAMES*

*Matthew R. Henry [I], †Songkil Kim [I], *Andrei G. Fedorov [I,II]*

*CORRESPONDING AUTHOR*

* AGF@gatech.edu

*AUTHOR ADDRESS*

[I] George W. Woodruff School of Mechanical Engineering, Georgia Institute of Technology, Atlanta, GA 30332, USA

[II] Parker H. Petit Institute for Bioengineering and Bioscience, Georgia Institute of Technology, Atlanta, GA 30332, USA

*PRESENT ADDRESS*

† School of Mechanical Engineering, Pusan National University, Busan 46241, South Korea

*CLASSIFICATION*

Physical Sciences – Applied Physical Sciences

ABSTRACT

A new state of radical thermal non-equilibrium in surface adsorbed molecules is discovered that enables rapid surface diffusion of energized adatoms with a negligible effect on the substrate surface temperature. Due to enhanced surface diffusion, growth rates can be achieved that improve the feasibility of many nanofabrication techniques. Since the adatom temperature cannot be directly measured without disturbing its thermodynamic state, the first principle hard-cube model is used to predict both the adatom effective temperature and the surface temperature in response to gaseous particle impingement in a vacuum. The validity of the approach is supported by local, spatially-resolved surface temperature measurements of the thermal response to supersonic microjet gas impingement. The ability to determine and control the adatom effective temperature, and therefore the surface diffusion rate, opens new degrees of freedom in controlling a wide range of nanofabrication processes that critically depend on surface diffusion of precursor molecules. This fundamental understanding has the potential to accelerate research into nanoscale fabrication and to yield the new materials with unique properties that are only accessible with nanoscale features.

SIGNIFICANCE STATEMENT

Gas jet impingement is used to activate strong non-equilibrium temperature states of adsorbed deposition precursor molecules on a vacuum surface. The Hard Cube Model (supported by experimental validation) is used to predict the effective adatom temperature, which can be applied to predict surface diffusion rates. Enhanced surface diffusion of adatoms is essential to efficient use of many nano-scale additive manufacturing techniques and gas impingement is a new method of growth acceleration.

KEYWORDS Surface Diffusion, Adsorption, Adatom Temperature, Sticking Coefficient, Hard Cube Model, Thermal Non-Equilibrium, Focused Electron Beam Induced Deposition

FUNDING This work was supported by the U.S. Department of Energy (DOE), Office of Science, Basic Energy Sciences (BES), under Award #DE-SC0010729.

ARTICLE

## 1) INTRODUCTION

Nanoscale features provide access to unique and useful material properties that are not available to bulk materials.[1,2] Three-dimensional additive nanomanufacturing down to an atomic scale structure and property control is enabled by Focused Electron/Ion Beam Induced Deposition (FEBID/FIBID).[3] Growth rate, which is a key consideration in nanomaterial deposition, is typically governed by the precursor supply rate of surface adsorbed precursor molecules to the deposition site.[4-6] The surface diffusion rate, which depends on the effective temperature of adsorbed molecules, is a critical consideration in enhancing the growth rate and resolution of FEBID, as well as many other nanoscale manufacturing techniques.[7] In fact, a higher surface diffusion rate of adatoms increases epitaxial growth rates[8] and improves deposition quality by preventing the dendrite formation that occurs in diffusion limited growth regimes.[9,10] In our previous work, control of adatom diffusion has been identified as the critical step towards localized, direct-write n-doping of graphene.[11] And non-equilibrium local thermal treatment of complex molecular clusters also opens interesting possibilities for driving self-organization patterning behavior, phase separation, and modifying the surface binding and electrochemical state of mono- and multi- layers deposited *via* ion soft landing.[12,13] Specifically, the structural re-arrangements of atomic/molecular ensembles linked through weak, non-covalent bonds may be altered using a locally induced state of thermal non-equilibrium through external stimulation via inert gas impingement, leading to directed molecular ordering and guided self-assembly.[14] Further, the diffusion rate can be modulated[15,16] to adjust the resulting deposit properties, such as porosity and grain size.[17] Conventionally, this is done by a bulk increase or decrease of temperature; however, recent experiments show that gas impingement at high

velocity onto the substrate in vacuum also modulates surface diffusion. What is intriguing is that in some cases gas impingement diminishes the adatom diffusion rate,[18,19] whereas in other cases gas impingement significantly enhances transport of adsorbed molecules.[9,20,21] Understanding of the fundamental mechanism for this shift in observed behavior is lacking, and it negatively impacts our ability to predict and control the nanostructure growth.

New modes of enhanced (or diminished) surface diffusion can be accessed *via* an externally applied thermally energized molecular beam that activates surface diffusion, without bulk heating of the substrate, by bringing adatoms into a state of strong thermal non-equilibrium with the surface. Since there is no way to directly measure the adatom temperature without perturbing its intrinsic thermodynamic state, the only alternative is to rely on the predictions using a suitable model that captures the key physics of interactions and validating it by comparison to carefully designed benchmark experiments. To this end, the conceptual framework of the classical hard-cube model (Figure 1.a) is adopted here but modified to include three interacting layers ("bodies") (Figure 1.b), such that the effective temperature of the "middle body", the adatom, may be determined. In the classical hard-cube model, the tangential velocity of an impinging particle is conserved, and the velocity normal to the surface is used in an elastic collision with a surface adsorption site to determine the post-collision particle energy. The original formulation of the hard-cube model predicts the sticking coefficient of precursor deposition molecules to the substrate by comparing the post-collision particle energy to the adsorption energy.[22,23] Here, we add an important new dimension to the model to enable prediction of the adatom and surface temperatures in response to energized gas impingement. Predictive power of the modified hard-cube model is verified by comparison to the microscopically local measurements of complex heating and cooling patterns of the substrate in response to supersonic gas jet impingement. The

use of the local jet can also bring the surface adsorbed precursor molecules into an excited thermodynamic state, far from equilibrium with the substrate surface, which is favorable for locally controlled nanofabrication. For example, modulation of the surface adsorbed precursor state by a supersonic inert gas jet in FEBID shows an enhancement of the surface adsorbed precursor diffusion rate (and therefore the nanostructure growth rate) by 10x,[20] which as we predict in this paper is indicative of substantially elevated adatom temperature with minimal impact on the substrate temperature. Predictions by the modified hard-cube model reveal the mechanism for bringing the molecular precursor to a state of thermal non-equilibrium with the surface with significant beneficial effects, such as enhanced growth rate and improved deposit morphology and structure for many nanofabrication techniques that rely on the optimal state of the surface adsorbed precursor.[24]

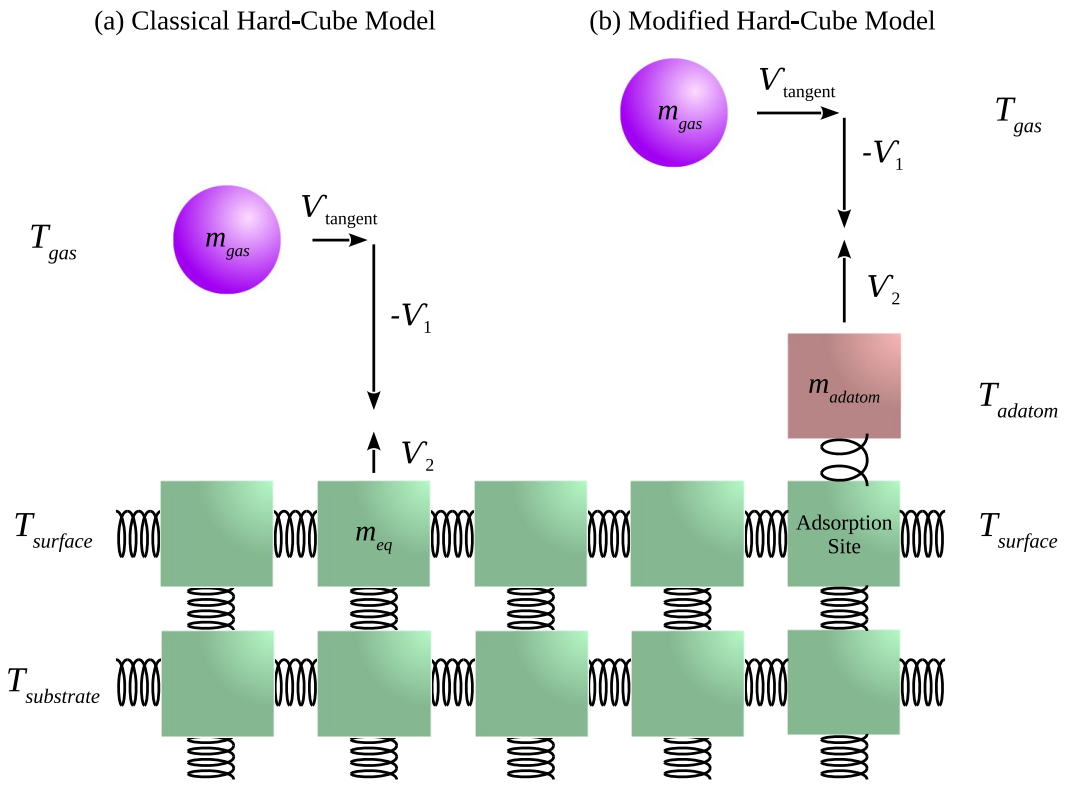

***Figure 1***: *(a) The classical hard-cube model is based on the elastic binary collision between the impinging particle and the impingement site modeled as a hard cube. Post-collision velocities are explicitly calculated from initial velocities by conservation of momentum and energy. Changes in impingement particle velocity determine the sticking coefficient and the heat flux to the adsorption site. (b) The modified hard-cube model applies the same approach between the impingement particle and adsorbed molecule and between the adsorbed molecule and the adsorption site.*

## 2) MATERIALS AND METHODS

### 2.1) Experimental Measurements of Surface Temperature

In order to validate the utility of the hard-cube model in determining the adsorption layer (adatom) temperature, its predictions of the surface temperature response to a gas jet are compared against spatially-resolved local temperature measurements. In vacuum, the magnitude of the thermal response is limited by the thermal conductivity of the substrate. Borosilicate glass, which has a low thermal conductivity, is selected to increase thermal sensitivity to gas impingement. A resistive thermal device (RTD) of dimensions 20$\mu m$ by 20$\mu m$ was fabricated on the substrate with deposition of a 10$nm$ chromium/35$nm$ platinum high electrical resistance serpentine pattern supported by low resistance legs, which is covered by a thin layer (~10$nm$) of silicon dioxide to protect the RTD from oxidation. The RTD response was calibrated in a controlled temperature oven, showing the expected linear behavior of metal electrical resistance vs temperature. During measurements, the substrate is mounted to a nano-scale positioning table in a scanning electron microscope (SEM) vacuum chamber such that the RTD position relative to the gas jet can be directly controlled as indicated in Figure 2.a and b. Data are collected in steps of 20$\mu m$ (equal to the effective size of the "measurement point") to map the thermal response

profile over the 2D surface. Measurement at each RTD position stabilizes to quasi-steady state in sub-second time, which indicates that the heat flux to the substrate and the far-field ambient temperature of the substrate can be considered steady-state at each data point.

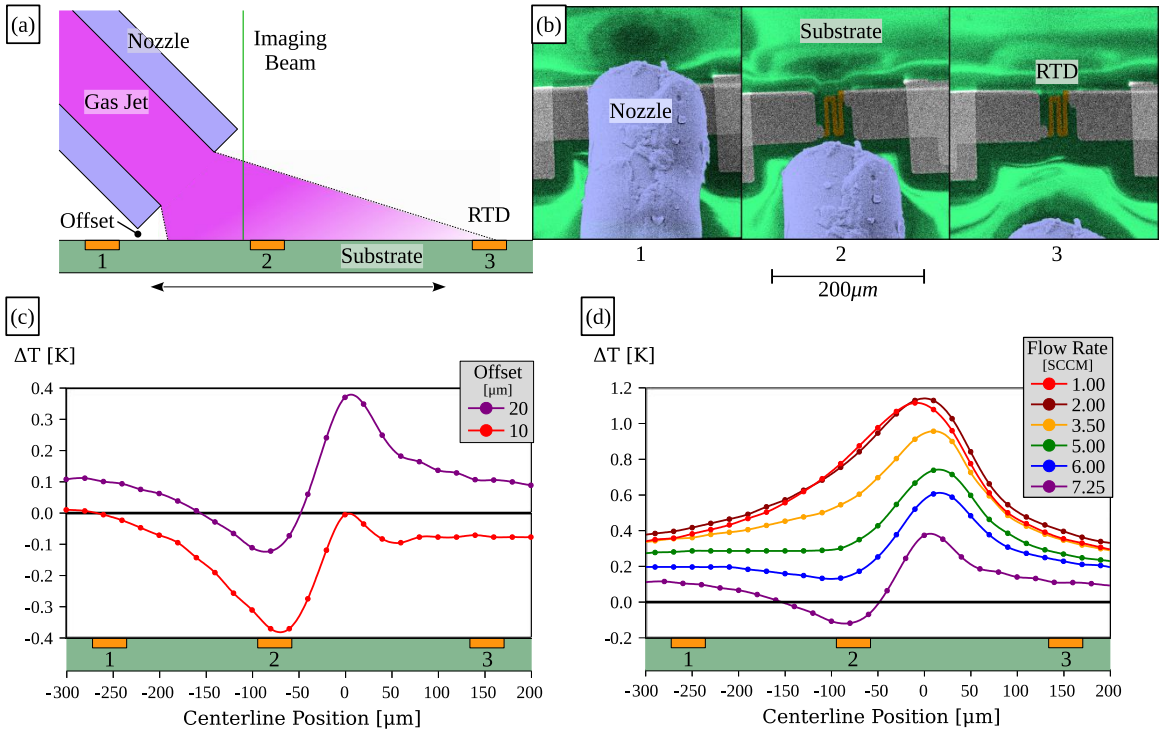


***Figure 2**: (a) A schematic side-profile of the RTD translation range illustrates how the RTD is positioned to collect thermal response data at different locations relative to the gas jet. (b) The SEM top-view image shows the RTD position as the substrate moves relative to the nozzle along the jet centerline position. The RTD thermal response (above the ambient equilibrium temperature when the jet is off) is collected for (c) a 7.25 ± 0.1 sccm oxygen gas jet with a 10μm and 20μm vertical offset between the nozzle tip outer diameter and the substrate and (d) an oxygen gas jet at various flow rates (in sccm) with a 20μm offset between the nozzle and the substrate. RTD temperature measurement uncertainty is ± 0.002K.*

During measurements, the gas jet nozzle is mounted at a 45° tilt from the surface normal and the 138$\mu m$ outer diameter edge is offset 20$\mu m$ above the substrate. Gas jet exits the 75$\mu m$ inner diameter nozzle at sonic velocity in the continuum choked flow regime at a stagnation temperature equal to the substrate far-field temperature. Detailed 2D surface maps of RTD measurements are collected for argon gas jets at 4.25 ± 0.14 and 7.00 ± 0.14 *sccm* flow rate with exit Knudsen numbers (defined by the ratio of the mean free path of gas molecules to the nozzle inner diameter) of 0.009 and 0.005, respectively, and an oxygen gas jet of 7.25 ± 0.1 *sccm* with a Knudsen number of 0.006 (Supporting Information). Representative centerline temperature profiles for the oxygen gas jet at varying flow rates are shown in Figure 2.c. The peak differential thermal response, defined relative to the equilibrium far field substrate temperature, occurs in the slip flow regime between 1.00 and 2.00 *sccm* with Knudsen numbers 0.04 and 0.02, respectively. At lower flow rates (not shown due to lesser relevance), the thermal response diminishes due to the diminished gas particle impingement rate to the substrate. At higher flow rates, the effect of isentropic acceleration is diminished due to the formation of a stagnation gas buffering region above the substrate surface. In Figure 2.d, centerline differential temperature profiles are presented for the oxygen gas jet of 7.25 *sccm* with vertical offsets of the nozzle tip from the substrate of 10$\mu m$ and 20$\mu m$. The thermal response profiles are comparable, but shifted by an average of 0.2$K$. The higher surface temperature at the greater offset distance is due to a slightly increased path length for isentropic expansion, resulting in the increased peak impingement velocity and increased kinetic energy delivered to the surface.

2.2) Prediction of Surface Temperature by the Hard-Cube Model in Combination with DSMC

In order to predict the surface temperature response to a gas jet, the distribution of gas particle impingement to the surface and the velocity distribution at each surface location must be

determined. The Direct Simulation Monte Carlo (DSMC) method was applied to simulate the gas flows for the experimental configurations. Each simulation compiled a log of every particle that impinged upon the substrate, its velocity orthogonal to the substrate, its location on the substrate, and its time of impact. This information is then sorted into finite substrate elements of $10\mu m \times 10\mu m$, based on the surface scanning step size used in the experiments, which provides the gas impingement rate for each substrate element. Particles in each element are then sorted into a velocity histogram. The expected form of a velocity distribution orthogonal to the substrate is $g(V_0) = c(-V_0)f(V_0)$ where $f(V_0)$ is the Gaussian distribution $\exp\left[-(V_0-\mu)^2/2\sigma_{gas}^2\right]/\sqrt{2\pi}\,\sigma_{gas}$, and it is weighted by a particle's orthogonal velocity $V_0$ towards the substrate. This equation is fitted to each sampled velocity histogram *via* least squares to obtain the distribution parameters $c$, $\mu$, and $\sigma$, where $\mu$ indicates the mean orthogonal velocity of gas and the standard deviation $\sigma$ indicates the gas temperature immediately above the substrate. The rate of impingement, mean orthogonal velocity, and gas temperature are used as the inputs to the hard-cube model to predict the substrate thermal response.[23]

The velocity distribution of gas particles adjacent to the substrate is defined by the Gaussian distribution based on the parameters obtained *via* DSMC. However, the particles that collide with a surface adsorption site are accelerated by addition of the adsorption energy $E_{ads}$ according to Equation 1.[23] With reference to Fig. 1, the probability distribution $g(V_1)$ of particles impinging upon the substrate can be expressed as $f(V_0)$ weighted by the relative velocity between a particle and a surface adsorption site (requiring that $V_2 > V_1$) and by the probability distribution $g(V_2)$ of the surface adsorption site velocities that are being impinged upon by gas particles, as indicated by Equation 2. By symmetry, $g(V_2)$ is given in Equation 3 where $f(V_2) = \exp\left[-V_2^2/2\sigma_{surface}^2\right]/\sqrt{2\pi}\sigma_{surface}$ is the Gaussian velocity distribution of surface adsorption sites

and $\sigma_{surface}$ is the standard deviation of velocity, which is dependent on the surface temperature $T_{surface}$ and its equivalent mass $m_{eq}$.

$$\frac{1}{2}M_1V_0^2 + E_{ads} = \frac{1}{2}M_1V_1^2 \quad (1)$$

$$g(V_1) = \int (V_2 - V_1) f(V_0) g(V_2) dV_2 \quad (2)$$

$$g(V_2) = \int (V_2 - V_1) f(V_2) g(V_1) dV_1 \quad (3)$$

Since a surface adsorption site is elastically coupled to the rest of the substrate, it is modeled by an equivalent mass somewhat greater than the actual adsorption site mass and is typically increased by a factor between one and two.[25] Earlier implementations of the classical hard-cube model used a factor of three.[22] Since this is the least defined parameter, its impact is considered in the uncertainty of all results. The post-collision velocity of the impinging particle is calculated in Equation 4 where $\mu$ is the ratio of impinging particle mass to the substrate hard-cube mass. This is used to determine how much energy is transferred to the substrate and whether the post-collision particle energy is greater than the adsorption energy. If the particle final energy is greater than $E_{ads}$, then the sticking coefficient is zero for the particular $V_1$ and $V_2$ pairing; otherwise it is one.[23] Integrating the energy delivered and the sticking coefficient across all surface adsorption site velocities and all impinging gas particle velocities provides both the average energy $E_{avg}$ delivered per particle (Equation 5) and the sticking coefficient $S$ at the given substrate element (surface site). The energy captured by the substrate due to a particle sticking is neglected because it is equal, on average, to the energy released in desorption when the rate of adsorption is equal to the rate of desorption (quasi-steady-state).

$$V_1^{\mathrm{I}} = \frac{\mu - 1}{\mu + 1}V_1 + \frac{2}{\mu + 1}V_2 \quad (4)$$

$$E_{avg} = \int\int 0.5M_1\left(V_1^2 - V_1^{*2}\right)g(V_1)g(V_2)dV_1dV_2 \quad (5)$$

In the case of single-layer adsorption, the fraction of occupied surface adsorption sites $\theta$ is given by Equation 6 where $P$ is the local impinging gas pressure, the rate constants of adsorption and desorption are $k_{ads} = r_{ads}/P(1-\theta)d$ and $k_{des} = r_{des}/\theta d$, respectively, and $d$ is the number of adsorption sites per unit area. The rates of adsorption $r_{ads} = S(1-\theta)(JA)$ and desorption $r_{des} = \theta Adv{\cdot}exp\left(-E_{ads}M_1/k_BT_{surface}\right)$ are defined in terms of the rate of gas particle impingement per unit area $J$, the site surface area $A$, and the desorption attempt frequency $v$.[23,26] Consolidating terms allows the fraction of occupied surface adsorption sites to be expressed as follows:

$$\theta = \frac{\left(k_{ads}/k_{des}\right)P}{1+\left(k_{ads}/k_{des}\right)P} \rightarrow \frac{SJe^{E_{ads}M_1/k_BT_{surface}}}{dv + SJe^{E_{ads}M_1/k_BT_{surface}}} \quad (6)$$

If the region of gas impingement to the surface is approximated as a disk of diameter $D$ and uniform surface temperature $T_{surface}$, then the rate $Q_2$ of thermal energy dissipated from that disk into the substrate is given by Equation 7 where $k$ is the thermal conductivity of the substrate material.[27] However, neither the temperature nor the impingement rate is uniform over the disk area. In order to compare the heat flux delivered by the gas jet to the heat flux dissipated into the substrate, analysis of each finite substrate element is considered as though the local impingement rate and the impingement velocity distribution are representative of the entire impingement region. The diameter of the equivalent disk region is calculated from the total area with an impingement rate greater than half the maximum jet impingement rate; this is approximately $100\mu m$ in our experiments. The rate $Q_1$ of energy delivered by the gas jet to the disk area (representing a specific finite surface element) is indicated in Equation 8. Since quasi-steady-state measurements are achieved within a sub-second response time of moving to a new finite

substrate element, $Q_1$ must equal $Q_2$, which allows prediction of the local surface temperature $T_{surface}$.

$$Q_2 = \underbrace{2D}_{\text{Shape Factor}} k(T_{surface} - T_{substrate}) \quad (7)$$

$$Q_1 = J\underbrace{(\pi D^2/4)}_{\text{Area}}\underbrace{(1-\theta)}_{\text{Available Sites}} E_{avg} \quad (8)$$

The thermal conductivity of the borosilicate glass substrate is $k = 1.2 W/mK$. The bulk number density of silicon dioxide groups is $n = 2.24 \times 10^{18} m^{-3}$, which yields the density of surface adsorption sites in the surface layer as $d = n^{2/3} = 7.93 \times 10^{18} m^{-2}$. The adsorption energies and vibrational frequencies are calculated based on the Lennard-Jones 12-6 potential parameters in Table 1, which is an appropriate model for closed-shell physisorption bonds. Specific pairings between components are calculated *via* the customary Lorentz-Berthelot mixing rules. The desorption attempt frequency is calculated by equating the parabolic term of the 12-6 potential curve to a spring model in order to identify the approximate spring stiffness $k_s = 72 E_{ads}/2^{1/3}$ $\sigma_{L\text{-}J}^2$ and the frequency $\upsilon = \left(k_S/m\right)^{1/2}/2\pi$.

**Table 1:** Lennard-Jones 12-6 Potential Parameters

| Material | Phase* | $E_{ads}$ [J] | $\sigma_{L\text{-}J}$ [$m$] |
|---|---|---|---|
| Silicon Dioxide[28] | S-S | $9.972\times10^{-22}$ | $3.265\times10^{-10}$ |
| Argon[29] | G-G | $1.654\times10^{-21}$ | $3.405\times10^{-10}$ |
| Oxygen[29] | G-G | $1.695\times10^{-21}$ | $3.382\times10^{-10}$ |
| Tungsten Hexacarbonyl[29] | G-G | $4.317\times10^{-21}$ | $3.400\times10^{-10}$ |
| *S-S denotes solid phase, G-G denotes gaseous phase | | | |

2.3) Assumptions and Limitations

We focus our attention on the most general case when the adatoms are weakly thermally coupled to the surface, i.e., the case of the adsorbate able to exist in externally-induced thermal non-equilibrium rather than being held in thermal equilibrium with the surface. The possibility of this thermally energized adatom state is evidenced by the fact that surface diffusion can be drastically enhanced with an inert gas jet impingement without significantly affecting the surface temperature.[20] The effective adatom temperature and the degree of thermal non-equilibrium relative to the surface depend on the relative influence of the particle impingement rate driving particle-adatom excitation versus the rate of adatom-surface thermal relaxation. To make problem analytically tractable, several simplifying assumptions are used for calculating the surface and adatom temperatures along with several approximations in treating the interlayer energy exchange. The first approximation is that tangential energy exchange between a particle and an adsorption site is negligible. This is generally considered to be true,[23] but becomes invalid when the tangential velocity component becomes significantly greater than the orthogonal component. The impingement collisions are considered to be fully elastic, and other modes of energy transfer are not expected due to the absence of appreciable surface heating and the absence of the impingement-induced adatom dissociation and chemical reactions. The adatom element corresponds to a monolayer; situations involving multi-layer adsorbates must account for the multiple layers and require the molecular dynamics simulations. The region of thermal response to the jet impingement is approximated as a disk in order to calculate the heat dissipation into the substrate. In treating a non-uniform temperature across the disk surface, lateral thermal interactions between adjacent adatoms are ignored (quasi-1D interactions), but accounting for 3D heat spreading by conduction from the disk impingement area into the

substrate. Each adatom element in the impingement zone is evaluated by assuming that its temperature and particle impingement rate can be represented as uniform over the entire area of the disk to be consistent with the treatment of uniform heat flux due to the spreading into the substrate across the entire disk.

2.4) Hard-Cube Model Validation

The RTD measured and hard-cube predicted surface temperature responses to the 7.00 *sccm* argon gas jet and 7.25 *sccm* oxygen gas jet are compared in Figure 3. The coupled DSMC-Hard-Cube predictions capture both the magnitude and complex features (transition between cooling and heating) of the surface RTD measurements. In the region farthest from the nozzle, the model predicts a $\Delta T$ that vanishes to zero, while the experimental results maintain a value of $0.2K$. In this region, the impingement rate is low, and no thermal response is expected. However, the gas is accelerated to its near terminal velocity, and the direction vector of mean velocity is nearly tangent to the surface. Consequently, the tangential velocity component that the hard-cube model neglects,[23] becomes the dominant contributor to surface thermal energy transfer, and its effect is not captured by the model due to its quasi 1D nature. In the region directly under the nozzle, the model and experimental measurements indicate a slight cooling effect. Particles that reach this region of the surface must depart from the jet centerline at an abrupt angle, resulting in a diminutive mean velocity as compared to other regions of the gas jet. Consequently, the temperature of gas particles is significantly reduced from the stagnation temperature. The resultant total root-mean-square velocity of impingement gas particles corresponds to a lower than ambient temperature, which cools the surface. The model results in Figure 3 are predictions for an equivalent mass factor of 1.5, and results generated with factors of one and two are

indistinguishable from the reported results, which indicates low sensitivity of the surface temperature on the equivalent mass of the surface adsorption site.

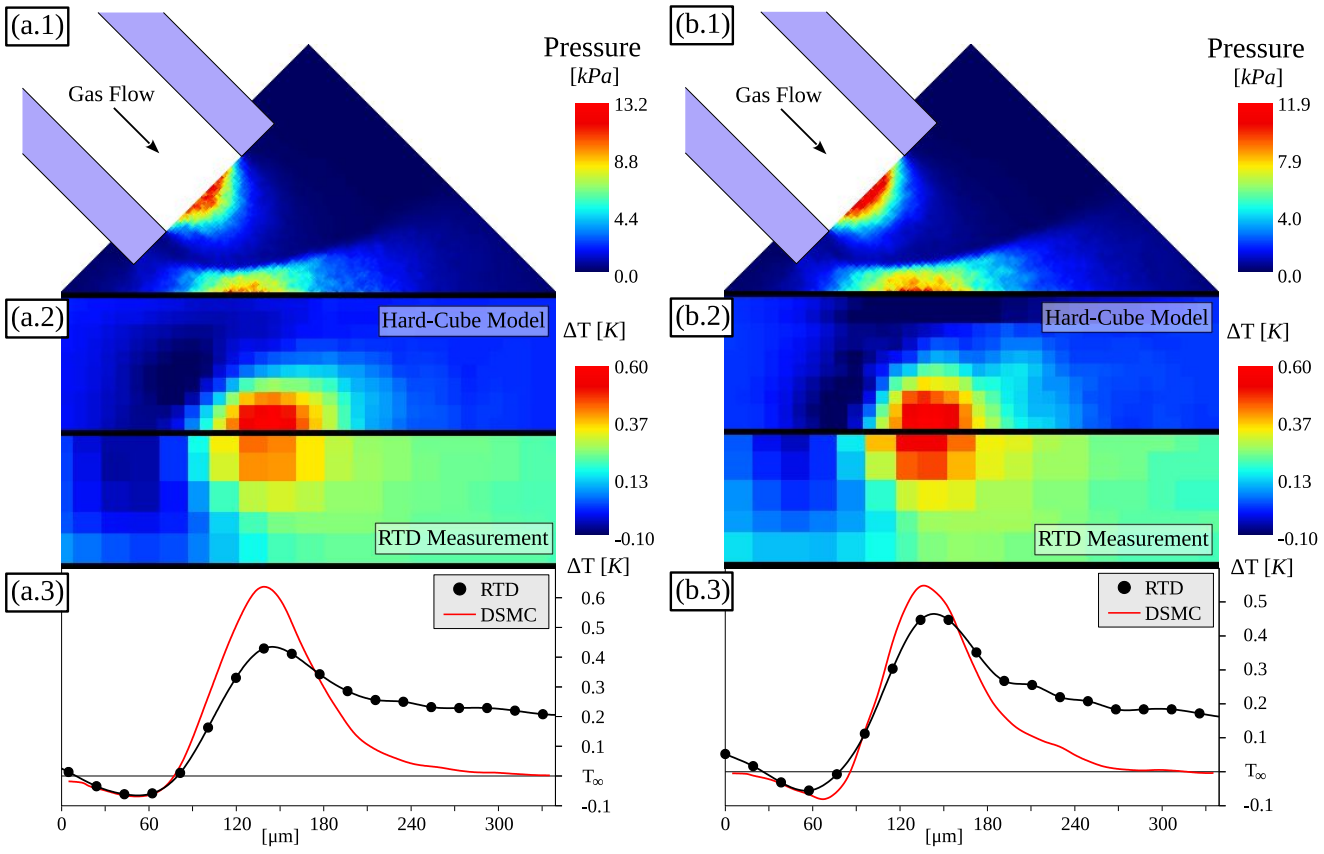


***Figure 3***: *RTD measurements and coupled DSMC-Hard-Cube model predictions are compared for (a) 7.00 ± 0.1 sccm argon gas jet and (b) 7.25 ± 0.1 sccm oxygen gas jet. (1) The cross-section view of the centerline pressure field from DSMC shows a stagnation gas cluster forming at the region of interest for heating and cooling at the surface. (2) Surface maps of the thermal response directly compare model predictions with RTD measurements. (3) Centerline profiles of the thermal response show that the model predictions capture the magnitude and behavior of the RTD measurements with the exception of the far-field deviation where 1-D hard-cube model is not valid. RTD temperature measurement uncertainty is ± 0.002K.*

2.5) Prediction of Adatom Temperature by the Modified Hard-Cube Model

The modified hard-cube model is next applied to predict the adsorption layer temperature. In the same manner that the surface temperature was determined by adjusting the adsorption site temperature such that the energy supplied by gas impingement and heat dissipated into the substrate are balanced, the adsorption layer temperature is determined by adjusting the adatom temperature such that the energy of impinging gas molecules transferred to the adsorption site is equal to the heat rejected from the adatom to the substrate. Thus, as indicated in Figure 1.b, the hard cube in the modified hard-cube model is the adsorbed molecule. Since the adatom is weakly bound to the substrate, its equivalent mass factor is one. The average energy, identified here as $E_1$, delivered to an adatom from a gas particle is given by Equation 5. The rate of energy delivered to the adatom depends on the average energy delivered per impingement particle $E_1$ and the impingement rate to the adatom $J$, as indicated in Equation 9.

$$q_1 = (J/d)E_1 \tag{9}$$

Regarding the thermal energy transfer from the adatom to the substrate, there are three possibilities. The first possibility is that the adatom undergoes an elastic collision with the substrate at a frequency $\upsilon$ corresponding to the adatom's vibrational frequency. This is a limiting case in which the high frequency of energy exchange forces the adatom to equilibrate to the surface temperature. However, in contrast to an impinging particle, which does undergo an elastic collision with the surface, an adsorbed particle oscillating at the trough of an energy well is not colliding with the surface. Since the adatom is expected to be in a highly non-equilibrium state relative to the surface, the vibrational energy exchanged between adatoms and the surface adsorption site is negligible relative to other factors. The second possibility is that the adatom exchanges no energy with the surface adsorption site. This is the other limiting case, in which the

adatom equilibrates with the impinging gas particles. In the third possibility, the impinging gas particles are driving adatoms to collide with adsorption sites at the frequency of gas particle impingement. These three possibilities are represented by Equation 10, where $E_2$ is the average hard-cube energy transfer from the adatom to the surface adsorption site as determined by Equation 5. Since the adatom is residing in the surface energy well, surface adsorption interactions cannot accelerate adatom motion and its Gaussian velocity $V_0$ distribution is therefore the same as that of the impinging particles, i.e. $V_1 = V_0$.

$$q_2 = \begin{cases} vE_2 & \text{Limit of } T_{adatom} = T_S \\ 0 & \text{Limit of Complete Decoupling} \\ (J/d)E_2 & \text{Impingement Driving Frequency} \end{cases} \quad (10)$$

As an example relevant to nanofabrication applications for e-beam direct-write of nanostructures (FEBID), the adsorption layer temperature is predicted for tungsten hexacarbonyl precursor molecules introduced with an argon carrier gas jet with the flow rate of 4.25 *sccm* as indicated in Figure 4. The predicted and measured surface excess temperatures $\Delta Ts$ are compared in Figure 4.b and c for the borosilicate glass substrate used in the hard-cube model validation experiments. In nanostructure growth experiments, a silicon dioxide layer is deposited on a silicon substrate ($k = 148^{W}/_{mK}$).[24] While the peak thermal response for such a substrate is predicted to be less than $0.01K$, the expected effective temperature of adsorbed tungsten hexacarbonyl is given in Figure 4.d, along with the predicted precursor sticking coefficient in Figure 4.e. Importantly, within the region of elevated gas particle impingement rate, the adatom experiences a significant temperature rise $\Delta T$ (anywhere between $35K$ and $130K$ depending on the strength of molecular interactions between the adsorbed molecules and substrate), which is consistent with the experimentally observed enhanced surface diffusion and an increase in the growth rate.[24] Outside this region, the adsorption layer temperature is predicted to drop below the

substrate temperature, suggesting diminished surface diffusion. However, due to the diminished impingement frequency outside the gas jet impact region, the adatom-surface relaxation is expected to become dominant over particle-adatom excitation, leading to rapid equilibration of the adatom and surface temperatures, which is a trivial limiting case of the hard-cube model application. Additionally, the applicability of the quasi-1D treatment of adatom-surface interactions diminishes in this region due to the increased significance of tangential velocity.

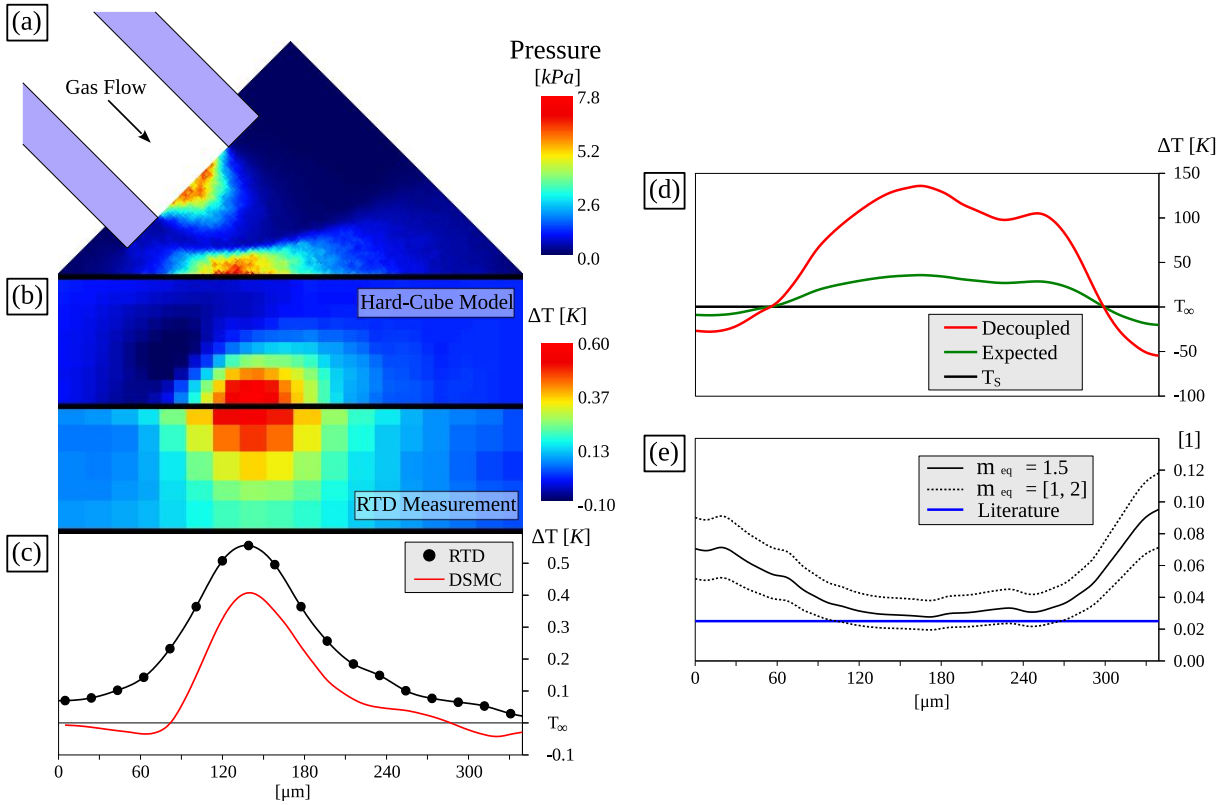


***Figure 4***: *(a) The cross-section view of the centerline pressure field predicted by DSMC for an argon jet at the flow rate 4.25 ± 0.14 sccm shows a stagnation gas cluster forming at the region of interest for heating and cooling at the surface. (b) Surface maps of the thermal response directly compare the modified DSMC-Hard-Cube model predictions with RTD measurements using the borosilicate glass substrate coated with a silicon dioxide surface layer. (c) Centerline profiles of the thermal response show that the model predictions capture the magnitude and*

*behavior of the RTD measurements. (d) The three possible scenarios for interaction strength between an adsorbed layer and the surface/substrate yield temperature predictions for tungsten hexacarbonyl adatoms, showing significant non-equilibrium between the substrate and adsorbed precursor molecules. (e) The sticking coefficient of tungsten hexacarbonyl onto silicon dioxide for an expected variation range of the surface adsorption site equivalent mass, showing an excellent agreement of the predicted sticking coefficient magnitude to the single-point measurement from the literature.[30] RTD temperature measurement uncertainty is ± 0.002K.*

When tungsten hexacarbonyl, a precursor for tungsten metal deposition, is injected as a minority species in a continuum flow carrier gas its particle velocities approximately match the carrier gas particle velocities.[31] Therefore, the argon jet impingement velocity distributions generated by DSMC are used to calculate the tungsten hexacarbonyl sticking coefficient *via* the hard-cube model. As indicated in Figure 4.e, the equivalent mass factor has a significant impact on the sticking coefficient but does not preclude meaningful estimation of the sticking coefficient. The sticking coefficient predicted *via* the hard-cube model is consistent with an experimentally determined sticking coefficient for tungsten hexacarbonyl on a silicon dioxide surface.[30]

## 3) CONCLUSIONS

In summary, we have developed a hybrid DSMC-Hard-Cube model for predicting the local temperature of an adsorbed layer suitable for application under non-equilibrium conditions. The model was verified through detailed microscopic measurements of the thermal response of a surface subjected to supersonic gas jet impingement in vacuum. Further, by considering data from the FEBID nanostructure growth experiments, we showed that the model can be applied to predict the effective adsorption layer temperature and its impact on the precursor molecular

surface diffusion rates. Since the predicted adatom temperature has little dependence on the equivalent mass factor, and all other parameters are readily determined from the first principles, the described method should enable making quantitative predictions for other solid/adsorbate pairs in vacuum with no use of empiricism. Using the model, we show that adatom heating by supersonic gas jet impingement creates a unique opportunity to access modes of enhanced surface diffusion without bulk substrate heating within a spatially confined domain, which is essential for achieving high growth rate and high resolution of additive nanofabrication. Ultimately, the ability to predict the sticking coefficient and adatom effective temperature (diffusion rate) can be combined with the precursor surface transport equation[4] to enable development of CAD tools for emerging atomic scale fabrication techniques.[3,5,6]

## SUPPORTING INFORMATION

The full 2D surface maps of the collected RTD measurements are available in the Supplementary Information.

## CONFLICTS OF INTEREST

There are no conflicts to declare.

## ABBREVIATIONS

DSMC, Direct Simulation Monte Carlo; FEBID, Focused Electron Beam Induced Deposition; FIBID, Focused Ion Beam Induced Deposition; RTD, Resistive Thermal Device; SEM, Scanning Electron Microscope.

## REFERENCES

1. Eremeyev VA. On Effective Properties of Materials at the Nano- and Microscales Considering Surface Effects. Acta Mech. 2016; 227: 29-42.

2. Hochella MF. Nanoscience and Technology: The Next Revolution in the Earth Sciences. Earth Planet. Sci. Lett. 2002; 203: 593-605.

3. Jesse S, Borisevich AY, Fowlkes JD, Lupini AR, Rack PD, Unocic RR, Sumpter BG, Kalinin SV, Belianinov A, Ovchinnikova OS. Directing Matter: Toward Atomic-Scale 3D Nanofabrication. ACS Nano. 2016; 10: 5600-5618.

4. Rykaczewski K, White WB, Fedorov AG. Analysis of Electron Beam Induced Deposition (EBID) of Residual Hydrocarbons in Electron Microscopy. J. Appl. Phys. 2007; 101: 054307.

5. Fowlkes JD, Winkler R, Lewis BB, Fernández-Pacheco A, Skoric L, Sanz-Hernández D, Stanford MG, Mutunga E, Rack PD, Plank H. High-Fidelity 3D-Nanoprinting via Focused Electron Beams: Computer-Aided Design (3BID). ACS Appl. Nano Mater. 2018; 1: 1028-1041.

6. Winkler R, Lewis BB, Fowlkes JD, Rack PD, Plank H. High-Fidelity 3D-Nanoprinting via Focused Electron Beams: Growth Fundamentals. ACS Appl. Nano Mater. 2018; 1: 1014-1027.

7. White WB, Rykaczewski R, Fedorov AG. What Controls Deposition Rate in Electron-Beam Chemical Vapor Deposition? Phys. Rev. Lett. 2006; 97: 086101.

8. Gao J, Zhang G, Zhang YW. Exploring Ag(111) Substrate for Epitaxially Growing Monolayer Stanene: A First-Principles Study. Sci. Rep. 2016; 6: 29107.

9. Jung DH, Kang C, Nam JE, Jeong H, Lee JS. Surface Diffusion Directed Growth of Anisotropic Graphene Domains on Different Copper Lattices. Sci. Rep. 2016; 6: 21136.

10. Ozhabes Y, Gunceler D, Arias TA. Stability and Surface Diffusion at Lithium-Electrolyte Interphases with Connections to Dendrite Suppression. Cornell University Library. 2015; arXiv:1504.05799v1.

11. Buchner F, Flechtner K, Bai Y, Zillner E, Kellner I, Steinrück H, Marbach H, Gottfried JM. Coordination of Iron Atoms by Tetraphenylporphyrin Monolayers and Multilayers on Ag(111) and Formation of Iron-Tetraphenylporphyrin. J. Phys. Chem. C. 2008; 112: 15458–15465.

12. Laskin J, Johnson GE, Warneke J, Prabhakaran V. From Isolated Ions to Multilayer Functional Materials Using Ion Soft-Landing. Angew. Chem. Int. Ed. 2018; doi:10.1002/anie.201712296.

13. Warneke J, McBriarty ME, Riechers SL, China S, Engelhard MH, Aprà E, Young RP, Washton NM, Jenne C, Johnson GE, Laskin J. Self-Organizing Layers from Complex Molecular Anions. Nat. Commun. 2018; DOI: 10.1038/s41467-018-04228-2.

14. Barth JV, Costantini G, Kern K. Engineering Atomic and Molecular Nanostructures at Surfaces. Nature. 2005; 437: 671-679.

15. Huang D, Xiao ZD, Gu JH, Huang NP, Yuan CW. TiO2 Thin Films Formation on Industrial Glass Through Self-Assembly Processing. Thin Solid Films. 1997; 305: 110-115.

16. Torrisia V, Ruffinob F. Nanoscale Structure of Submicron-Thick Sputter-Deposited Pd Films: Effect of the Adatoms Diffusivity by the Film-Substrate Interaction. Surf. Coat. Tech. 2017; 315: 123-129.

17. Vicka D, Friedricha LJ, Dewa SK, Bretta MJ, Robbiea K, Setoa M, Smy T. Self-Shadowing and Surface Diffusion Effects in Obliquely Deposited Thin Films. Thin Solid Films. 1999; 339: 88-94.

18. Barwicz T, Cohen GM, Reuter KB, Bangsaruntip S, Sleight JW. Anisotropic Capillary Instability of Silicon Nanostructures Under Hydrogen Anneal. Appl. Phys. Lett. 2012; 100: 093109.

19. Day RW, Mankin MN, Gao R, No YS, Kim SK, Bell DC, Park HG, Lieber CM. Plateau–Rayleigh Crystal Growth of Periodic Shells on One-Dimensional Substrates. Nat. Nanotechnol. 2015; 10: 345-352.

20. Henry MR, Kim S, Rykaczewski K, Fedorov AG. Inert Gas Jets for Growth Control in Electron Beam Induced Deposition. Appl. Phys. Lett. 2011; 98: 263109.

21. Kim S, Russell M, Henry M, Kim SS, Naik RR, Voevodin AA, Jang SS, Tsukruk VV, Fedorov AG. Dynamic Modulation of Electronic Properties of Graphene by Localized Carbon Doping Using Focused Electron Beam Induced Deposition. Nanoscale. 2015; 7: 14946-14952.

22. Grimmelmann EK, Tully JC, Cardillo MJ. Hard-Cube Model Analysis of Gas-Surface Energy Accommodation. J. Chem. Phys. 1980; 72: 1039.

23. Kolasinski K. Surface Science – Foundations of Catalysis and Nanoscience. John Wiley & Sons: Chichester, 2012; pp 112, 133, 173.

24. Henry M, Kim S, Fedorov AG. High Purity Tungsten Nanostructures via Focused Electron Beam Induced Deposition with Carrier Gas Assisted Supersonic Jet Delivery of Organometallic Precursors. J. Phys. Chem. C. 2016; 120: 10584–10590.

25. Arumainayagam CR, Schoofs GR, McMaster MC, Madix R J. Dynamics of Molecular Adsorption of Ethane with Pt(111): A Supersonic Molecular Beam Study. J. Phys. Chem. 1991; 95: 1041-1047.

26. Masel RI. Principles of Adsorption and Reaction on Solid Surfaces; John Wiley & Sons: New York, 1996; pp 240-241.

27. Nellis G, Klein S. Heat Transfer; CUP: New York, 2009; pp 204.

28. Talu O, Myers AL. Reference Potentials for Adsorption of Helium, Argon, Methane, and Krypton in High-Silica Zeolites. Colloids Surf. A. 2001; 187-188: 83-93.

29. Bernardes CES, Lopes JNC, Piedade MEM. All-Atom Force Field for Molecular Dynamics Simulations on Organotransition Metal Solids and Liquids. Application to M(CO)n (M = Cr, Fe, Ni, Mo, Ru, or W) Compounds. J. Phys. Chem. A. 2013; 117 11107–11113.

30. Fowlkes JD, Rack PD. Fundamental Electron-Precursor-Solid Interactions Derived from Time-Dependent Electron-Beam-Induced Deposition Simulations and Experiments. ACS Nano. 2010; 4: 1619-1629.

31. Raghuraman P, Davidovits P. Velocity Slip of Gas Mixtures in Free Jet Expansions. Phys. Fluids. 1978; 21: 1485-1489.